Large-Scale Label-Free Comparative Proteomics Analysis of Polo-Like Kinase 1 Inhibition via the Small-Molecule Inhibitor BI 6727 (Volasertib) in BRAF^V600E Mutant Melanoma Cells

Brian D. Cholewa,[†,‡] Molly C. Pellitteri-Hahn,[§] Cameron O. Scarlett,[§] and Nihal Ahmad*[,†,‡,‖]

[†]Department of Dermatology, [‡]Molecular and Environmental Toxicology Center, and [§]School of Pharmacy, University of Wisconsin, 1300 University Avenue, Madison, Wisconsin 53706, United States

[‖]William S. Middleton Memorial VA Hospital, 2500 Overlook Terrace, Madison, Wisconsin 53705, United States

S *Supporting Information*

ABSTRACT: Polo-like kinase 1 (Plk1) is a serine/threonine kinase that plays a key role during the cell cycle by regulating mitotic entry, progression, and exit. Plk1 is overexpressed in a variety of human cancers and is essential to sustained oncogenic proliferation, thus making Plk1 an attractive therapeutic target. However, the clinical efficacy of Plk1 inhibition has not emulated the preclinical success, stressing an urgent need for a better understanding of Plk1 signaling. This study addresses that need by utilizing a quantitative proteomics strategy to compare the proteome of BRAF^V600E mutant melanoma cells following treatment with the Plk1-specific inhibitor BI 6727. Employing label-free nano-LC–MS/MS technology on a Q-exactive followed by SIEVE processing, we identified more than 20 proteins of interest, many of which have not been previously associated with Plk1 signaling. Here we report the down-regulation of multiple metabolic proteins with an associated decrease in cellular metabolism, as assessed by lactate and NAD levels. Furthermore, we have also identified the down-regulation of multiple proteasomal subunits, resulting in a significant decrease in 20S proteasome activity. Additionally, we have identified a novel association between Plk1 and p53 through heterogeneous ribonucleoprotein C1/C2 (hnRNPC), thus providing valuable insight into Plk1's role in cancer cell survival.

KEYWORDS: *polo-like kinase 1, Plk1, proteomics, hnRNPC, p53, LDHA, proteasome, glycolysis, melanoma, BI 6727*
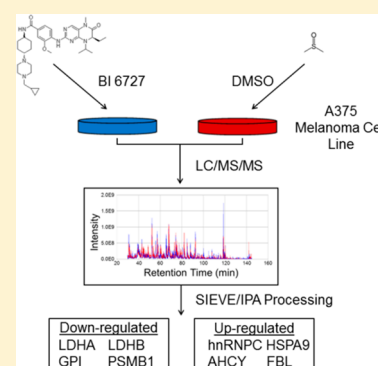
INTRODUCTION

Polo-like kinase 1 (Plk1) is the most well-studied member of the polo-like family of kinases and is most commonly known for its regulatory role during mitosis, where it has been shown to be a critical component of centrosome maturation, kinetochore–microtubule attachment, bipolar spindle formation, and cytokinesis.[1−4] The overexpression of Plk1 is common in aberrant cells and has been identified in roughly 60% of reported cancers including melanoma, breast, ovarian, thyroid, colon, prostate, pancreatic, head and neck, nonsmall cell lung, and non-Hodgkin's lymphomas.[5−13] Furthermore, the overexpression of Plk1 has been linked to poor disease prognosis and a decreased survival rate.[14,15] In vitro studies have shown that specific inhibition of Plk1 can significantly reduce the proliferation and viability of multiple melanoma cell lines by inducing G2/M phase cell cycle arrest and mitotic catastrophe without detriment to normal adult or neonatal human epidermal melanocytes (HEMs).[9] These data have made Plk1 an attractive target for small-molecule inhibition and provoked the development of over a dozen Plk1 inhibitors, six of which have gone to clinical trials.[16−21] However, despite Plk1 inhibition having great preclinical success for cancer treatment, the clinical potential of Plk1-targeted inhibition for human cancers has yet to be realized. This emphasizes the need for a more in-depth understanding of Plk1 signaling in cancer. This study addresses that need by employing a large-scale comparative proteomics analysis to examine the downstream effects of Plk1 inhibition using the small-molecule inhibitor BI 6727.

BI 6727 (Volasertib) is a second-generation Plk1 inhibitor and is currently the most specific Plk1 ATP-competitive inhibitor commercially available with an IC$_{50}$ of 0.87 nM.[22] Plk1 inhibition by BI 6727 has been shown to have potent antitumorigenic activity in multiple preclinical studies, but the downstream mechanism by which BI 6727 confers its therapeutic effect remains largely undefined. In an effort to identify novel regulatory effects of Plk1 inhibition in melanoma, we used a label-free, relative quantitation strategy to compare the proteomes of A375 melanoma cells cultured in the presence or absence of BI 6727. The A375 melanoma cell line has been reported to express high levels of Plk1 when compared with HEMs and is sensitive to the targeted depletion of Plk1.[9]

Furthermore, A375 cells harbor the BRAF[V600E] mutation, a mutation present in roughly 50% of melanoma cases, thus making it an ideal candidate for our proteomics analysis.[23]

Our comparative proteomics strategy was conducted by employing data-dependent nano-LC−MS/MS analysis on a Q-Exactive with the resultant data being searched against the human proteome using the Sequest search engine and further analyzed with the SIEVE software package to reveal proteins with altered expression. This analysis resulted in the positive identification of 1819 proteins (≤1% false discovery rate (FDR)), 343 of which had significantly altered expression. Using ingenuity pathway analysis (IPA) to filter the data under more stringent conditions, we identified a subset of 23 proteins that were significantly altered due to BI 6727 inhibition of Plk1, most of which have no previously reported associations with Plk1. Importantly, we have identified proteins involved in cellular metabolism, proteasomal degradation, and p53 translation, thus providing novel insight into Plk1's role in cancer cell survival.

■ MATERIALS AND METHODS

Cell Culture

A375 human melanoma cells (ATCC, VA) were cultured in HyClone Dulbecco's modified Eagle's medium (DMEM, Thermo, CA) supplemented with 10% fetal bovine serum (FBS, Thermo, CA). Cells were maintained in a humidified incubator with 5% CO_2 at 37 °C.

BI 6727 Treatment

1×10^6 A375 human melanoma cells (ATCC, VA) were seeded in 100 mm tissue culture plates (TPP, MO) containing 10 mL of supplemented DMEM (Thermo, CA) and were allowed to recover in untreated medium for 24 h under standard cell culture conditions. Following recovery, medium was aspirated, and cells were treated with 25 nM BI 6727 (Chemietek, IN) or vehicle control (DMSO) in supplemented DMEM. After 24 h, cells were collected by trypsin digestion and centrifugation at 300g for 3 min at 4 °C. Supernatant was removed and cell pellets were washed three times with PBS. The treatments were performed using identical procedures on two varying A375 cell passages three times each for a total of six experimental replicates per treatment group. Cell pellets were stored at −80 °C prior to cell lysate preparation.

Cell Lysate Preparation for Proteomics Analysis

Cell pellets were lysed mechanically with a needle in the absence of protease inhibitors or lysis buffer according to the following protocol. 0.3 mL of ice cold PBS was added to frozen cell pellets, and the resulting mixture was lysed by passing through a 23 gauge needle 15 times. The cytosolic protein fraction was isolated by centrifugation at 10 000g for 10 min at 4 °C to remove cellular debris. Protein concentration of the extracts was measured by MicroBCA assay (Thermo Fisher Scientific, IL). A total of 20 μg of protein from each of the six replicates (control and treated) was digested with 1 μg of sequencing grade trypsin (Promega, Fitchburg, WI). Following an overnight digestion at 37 °C samples were acidified with 10% formic acid and prepared for LC−MS/MS by C18 Zip-Tip purification according to the manufacturers protocol (Millipore, Billerica, MA). Peptide samples were resuspended in water with 0.1% formic acid (v/v) and analyzed by nano-LC−MS/MS.

MS/MS Protein Identification and Quantification

For label-free, relative, quantitative analysis, six replicates of each sample were analyzed by nano-LC−MS/MS. For each run, 1 μg of the digest was injected on a 100 μm × 100 mm, reverse-phase C18 BEH column with 1.7 um particles and a 300 Å pore size (Waters, Milford, MA) using a Waters nanoAcquity system. Chromatography solvents were water (A) and acetonitrile (B), both with 0.1% formic acid. Peptides were eluted from the column with the following gradient 3 to 35% B (130 min). At 140 min, the gradient increased to 95% B and was held there for 10 min. At 160 min, the gradient returned to 3% to re-equilibrate the column for the next injection. A short 50 min linear gradient blank was run between samples to prevent sample carryover. Peptides eluting from the column were analyzed by data-dependent MS/MS on a Q-Exactive Orbitrap mass spectrometer (Thermo Fisher Scientific, MA). A top-15 method was used to acquire data. In brief, the instrument settings were as follows: resolution was set to 70 000 for MS scans and 17 500 for the data-dependent MS/MS scans to increase speed. The MS AGC target was set to 10^6 counts, while MS/MS AGC target was set to 10^5. The MS scan range was from 300 to 2000 m/z. MS scans were recorded in profile mode, while the MS/MS was recorded in centroid mode, to reduce data file size. Dynamic exclusion was set to a repeat count of 1 with a 25 s duration.

Data Processing

Following LC−MS/MS acquisition, the data were searched using Sequest HT Proteome Discoverer 1.4 search engine (Thermo Fisher Scientific), against the Uniprot Human database (6/23/2013, 20 209 sequences) at a false discovery cut off ≤1%. Following protein identification, the LC−MS/MS data were aligned using Chromalign. Quantitation of peptides eluting between 38 and 145 min was performed on the processed data using SIEVE 2.1 (Thermo Fisher Scientific), which uses MS intensities from raw LC−MS data to find statistical proteomic differences between two samples. Prior to ratio quantitation in SIEVE, peak intensities from all 12 LC−MS/MS runs were normalized by the total ion chromatogram intensity. Statistical filters were set to assess the quality of the data. Proteins ratios calculated had to be significant with a p value lower than 0.05, and the CV raw MS intensities of the six replicates had to be within 30%. This helped minimize the effect of run-to-run variability.

Data Analysis

Identified proteins from the SIEVE processing were initially analyzed and filtered using IPA (Ingenuity Systems, CA) under a trial license. A data set containing proteins with only uniquely identified amino acid sequences (peptides) with a high level of confidence ($p < 0.05$) was uploaded into IPA with number of peptides identified, triggered MS/MS fragmentation scans (hits), and the corresponding ratio (treated/untreated) set as the observational parameters with Swiss-Prot accession numbers used for gene ID. A secondary data set was then generated using IPA filters set to proteins with more than two identified peptides on no fewer than four hits with a greater than two-fold change in expression. Another secondary data set was generated using the IPA connect tool to identify any Plk1-associated proteins with an expression change greater than two-fold. The two secondary data sets were combined, and their molecular function and biological processes were assessed using PANTHER (Protein ANalysis THrough Evolutionary Relationships).

Western Blot Analysis

5×10^5 A375 cells were plated and grown in a 10 cm culture dish and treated with BI 6727 at 25 nM, 100 nM, or vehicle control, as previously described. Following 24 h treatment, cells were trypsinized, washed with ice-cold PBS, and lysed with RIPA buffer (50 mM Tris, 150 mM NaCl, 1% NP-40, 0.5% deoxycholic acid, 0.1% SDS) with phenylmethylsulfonyl fluoride (PMSF) and protease inhibitor cocktail (Pierce, IL). Protein concentration was measured with BCA Protein Assay (Pierce, IL). For immunoblot analysis, 30 μg of protein was subjected to sodium dodecyl sulfate polyacrylamide gel electrophoresis (SDS-PAGE) using Mini-PROTEAN TGX precast gels and transferred onto nitrocellulose membrane. Blots were blocked in 5% nonfat dry milk in tris-buffered saline +0.1% tween-20 (TBST), followed by probing with desired primary antibodies: anti-LDHA, AurkB, p53, β-actin (Cell Signaling nos. 2012, 3094, 9282, 4970), PSMB1, PSMB2, or PSMB5 (Abcam nos. ab135830, ab166628, ab3330). Blots were then incubated with the appropriate HRP-conjugated antibodies followed by chemiluminescent detection (Pierce, IL).

Quantitative Real-Time PCR

5×10^5 A375 cells were plated and grown in a 10 cm culture dish and treated with BI 6727 at 25 nM, 100 nM, or vehicle control, as previously described. Following 24 h of treatment, cells were trypsinized and washed with ice-cold PBS, followed by RNA isolation using the RNeasy plus mini kit (Qiagen, CA) and first strand cDNA created with M-MLV reverse transcriptase (Promega, WI) according to vendor's protocol. Quantitative real-time RT-PCR was performed in triplicate in 20 μL reactions with SYBR Premix Ex Taq Perfect Real Time (Takara, WI) with 100 ng first-strand cDNA and 0.2 μg of each desired primer pair. The sequences for GPI, LDHB, and p21 (PrimerBankID 296080692c3, 291575126c2, 310832423c1) were acquired from the PrimerBank online database.[24] Samples were cycled once at 95 °C for 10 min, then 35 cycles of 95, 58, and 72 °C for 5, 15, and 20 s, respectively. Relative mRNA was calculated using the $\Delta\Delta C_T$ method with GAPDH as an endogenous control.

Lactate Assay

For lactate assay, 8×10^3 A375 cells were plated and grown in a 96-well plate and treated with BI 6727 at 25 nM, 100 nM, or vehicle control, as previously described. 24 h following treatments, 500 μL of spent media was removed from each group and immediately cleared of LDH proteins by centrifugation in 10 kDa molecular weight cutoff spin columns and stored at −80 °C. All samples were diluted by adding 10 μL of media to 90 μL of lactate assay buffer and subsequently used in a serial dilution containing a final concentration of either 1, 0.5, 0.25, or 0.125% media in lactate assay buffer with a final volume of 50 μL in black 96-well half area plates (Corning, MA). Lactate assay was performed per manufacturer's protocol, and fluorescence intensity was measured on the Biotek Synergy H1 microplate reader at $\lambda_{ex} = 535/\lambda_{em} = 587$.

NAD, NADH, and NADPH Assays

3×10^3 A375 cells were plated and grown in 96-well half-volume white-wall plates (Corning, MA) and treated with BI 6727, as previously described. Following 24 h treatments, samples were processed using the NAD(P)H-Glo detection system (Promega, WI) or NAD/NADH-Glo assay (Promega, WI) as per manufacturer's protocol. Luminescence was detected using the Biotek Synergy H1 microplate reader.

20S Proteasome Activity Assay

For assessing 20S proteasome activity, A375 cells were treated with BI 6727 at 25 nM, 100 nM, or vehicle control, as previously described. Following 24 h treatments, cells were lysed in 50 μL of ice-cold RIPA buffer for 10 min at room temperature while shaking. Next, 25 μL of lysate was added to a 96-well plate containing BCA reagent (Pierce, Rockford, IL) and incubated at 37 °C for 30 min, while 10 μL of lysate was added to the 20S Proteasome Activity Assay (Millipore, MA) prepared per manufacturer's protocol and incubated at 37 °C for 2 h. Relative levels of protein were quantified using the BCA assay absorbance detected using the Biotek Synergy H1 microplate reader at 562 nm. 20S proteasome activity was quantified using fluorescence intensity on the Synergy H1 microplate reader at $\lambda_{ex} = 380/\lambda_{em} = 460$. Proteasome activity was then normalized to relative protein concentration, and the mean of relative activity for each treatment ($n = 6$) was represented graphically.

Immunofluorescence Staining

For immunofluorescence staining, cells were plated and grown on BD Falcon CultureSlides (BD Biosciences, San Jose, CA) and treated with BI 6727 as previously described. The cells were fixed with a 4% paraformaldehyde in PBS (pH 7.1) for 15 min at room temperature, then blocked with 5% normal goat serum in 0.3% Triton X-100 for 1 h. After blocking, cells were incubated overnight in anti-β-tubulin primary antibody in blocking buffer (1:100, Cell Signaling no. 2128), followed by a secondary incubation with Alexa Fluor 594 antirabbit IgG antibody in blocking buffer (5 μg/mL, Invitrogen no. A-11037) for 1 h in the dark. The cells were then counter-stained with Hoecsht 33342 (Invitrogen, Grand Island, NY) for nuclear staining, and a ProLong antifade kit was applied per vendor's protocol (Molecular Probes, Eugene, OR). Slides were examined under a Nikon Ti microscope using the respective manufacturer's suggested filter sets.

Cell Cycle Analysis

1×10^5 A375 cells were plated and grown in a six-well tissue culture dish (TPP, CHE) and treated with BI 6727, as previously described. Following treatment, cells were trypsinized for 5 min and transferred to 5 mL Falcon tubes containing cultured media. Samples were centrifuged at 1000 rpm for 2 min, and the supernatant was aspirated prior to the cells being resuspended in ice-cold 100% ethanol added dropwise while gently vortexing. Samples were stored at −20 °C overnight prior to centrifugation and resuspension in 500 μL of propidium iodide (PI) buffer (PBS, 50 μg/mL PI, 0.1 mg/mL RNase A, 0.05% Triton-X). Samples were incubated at 37 °C for 40 min in dark and stored at 4 °C until processed by flow cytometry in the FL-2A channel. Cell cycle analysis was done using ModFit LT software (Verity Software, Topsham, ME).

■ RESULTS AND DISCUSSION

BI 6727 Treatment, Protein Identification, Quantification, and Analysis

In an effort to identify the downstream molecular mechanisms of Plk1 in melanoma, we elucidated quantitative changes in the proteome of human melanoma cells following Plk1 inhibition with BI 6727. Data acquired by nano-ESI−MS/MS on a Q-Exactive spectrometer were processed with SIEVE software to reveal up- or down-regulated proteins following Plk1 inhibition.

To determine the most effective concentration of BI 6727, we assessed A375 cell viability following a defined range of BI 6727 treatments (0.1−1000 nM, data not shown). We determined 25 nM of BI 6727 as the lowest effective concentration to cause a statistically significant decrease in cell viability after 48 h. To assess the molecular functions that contribute to the reduction of A375 cell viability, we terminated treatments after 24 h to limit the necrotic and late apoptotic cell population.

Several methods for relative proteomic quantitation have been described.[25−27] Labeling methods, including chemical modification approaches (I-Traq, etc.) and stable isotope labeling, can be expensive but generally require fewer LC−MS runs to generate robust results. Label-free approaches are becoming more popular as improvements in instrumentation (resolution and mass accuracy), and improvements in data analysis software facilitate analysis of large data sets. The capabilities of our Q-Exactive spectrometer made a label-free approach attractive. The high scanning speed coupled to the resolving power and mass accuracy of the Q-Exactive Orbitrap make it particularly useful for accurate, label-free, quantitative protein analysis. This is primarily due to the higher resolution (smaller diameter) Orbitrap cell of the Q-Exactive. High-resolution and mass accuracy facilitate area-under-the-curve analysis with the SIEVE software by allowing accurate tracking of peptides through their chromatographic elution. Additionally, the improvement in resolution allows shorter transient acquisitions. This improves the duty cycle and allows for increased peptide identification at the MS/MS level. The Q Exactive has been shown to identify a higher number of compounds with better confidence in multiple comparison studies.[28−30] Thus, there is greater proteome coverage, which enhances the ability to quantitate lower abundant proteins than is achieved with spectral-counting approaches.[31−36] Indeed, the power of this combination of instrumentation and software was born out in the ability of our analysis to positively identify over 1800 proteins, at a cutoff of ≤1% FDR, with 343 of these identified proteins showing significantly altered expression (Tables S1 and S2 in the Supporting Information).

A key step in label-free quantitative proteomic analysis is the evaluation of run-to-run and sample-to-sample reproducibility/variability.[37] Prior to the full analysis, we performed a pilot study of BI 6727-treated cells and control replicates, using identical sample preparation and LC−MS parameters as previously described to assess variability. Two A375 human melanoma aliquots were seeded in 100 mm tissue culture plates as previously described and grown for 24 h under standard cell culture conditions. Both plates were lysed and digested as laid out in our methods. Two replicate injections of 1 μg of both control and treated samples were run. Resulting data were subject to SEQUEST searches against Uniprot Human at ≤2% FDR, using Proteome Discoverer. A higher FDR was used in assessing the run-to-run variability to delve deeper into the data. These four control runs had an average of 715 proteins identified, with an average of 1500 unique peptides and over 3100 total scans. Percent overlap between the two control biological replicates was 67% at the protein level and 55% at the peptide level (data not shown). Not surprisingly, percent overlap of the duplicate injections was higher with 70% overlap at the protein level and 62% at the peptide level (data not shown). Percent overlap between both injection and biological replicates is consistent with a recent review article highlighting the strengths and limitations of label-free proteomic quantification.[37] Our control runs emphasize the need for

more than three experimental replicates of each sample type to accurately determine protein ratios in label-free studies. To maximize the statistical power of our analysis, we opted to analyze six replicates of control versus Plk1 treated A375 cells.

The first step in any direct comparison of treated versus control samples MS peak intensity is alignment of base peak chromatograms. SIEVE uses Chromalign, a proprietary algorithm to align the data. Chromalign evaluates the quality of alignment between samples by assigning a score. Alignments with scores above 0.75 are considered acceptable for further quantitative analysis. Our data showed average alignment scores of 0.825, with the treatment groups clustering together (Figure 1A). Because SIEVE, like many other label-free methods, allows for conserved peptides to be equally considered for all candidate proteins, we decided to take the approach of only quantitating unique peptides. This avoids inaccurate fold-change calculations due to differential regulation of proteins sharing a conserved peptide. The Q-Exactive's speed, was key in being able to take this stringent approach to label-free
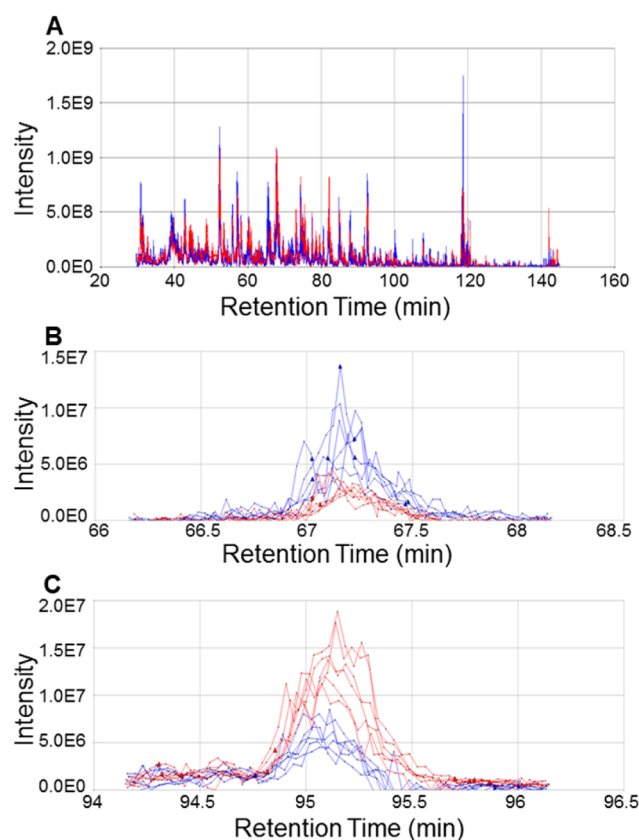

Figure 1. Relative quantitation chromatograms. (A) For label-free relative quantitation, six replicates of the tryptic digests were analyzed. The chromatograms were aligned using SIEVE 2.1. An overlay of the base peak chromatograms of control (blue) and treated (red) samples shows good alignment and comparable loading in the region of peptide elution (38−145 min RT). (B) An example of a peptide that is down-regulated in response to treatment. Shown is a SIEVE-aligned, extracted-ion chromatograms for peptide 524.9481 *m/z* (metastasis-associated protein). Triangles indicate where MS/MS identification scans were triggered. (C) Example of a peptide that is up-regulated in response to treatment. Shown is a SIEVE-aligned, extracted-ion chromatogram for peptide 373.3691 *m/z* (PH-domain leucine-rich protein). Triangles indicate where MS/MS identification scans were triggered.

proteomics. Label-free quantitation approaches do not rely on internal standards, and thus care needs to be taken to accurately filter the data to reproducibly quantitate proteins. SIEVE allows for calculated peptides ratios between samples to be filtered not only on p value using Fisher's combined probability but also based on variation in the MS peak intensities between the experimental replicates. After data were normalized to the total ion current (TIC), we filtered all protein ratios to have a CV between the six replicates (25 nM BI 6727 or vehicle control) to be ≤30%. Peptides had to show up in all six replicates of a treatment at the MS level to be quantitated (Figure 1B,C). This stringent filter allows us to have additional confidence in our data. One of the benefits SIEVE has over spectral counting is as long as a peptide has a consistent MS peak, it only has to be positively identified once to determine its ratio. Thus, we were able to identify lower abundant proteins using our approach. Finally, peptide fold-change ratios had to be significant at a p value of ≤0.05 to be considered in our analysis.

Our protein analysis was initially done using IPA. A data set containing proteins with only uniquely identified peptides with a high level of confidence ($p < 0.05$) was uploaded into IPA with the number of peptides identified (Figure 2A) and the
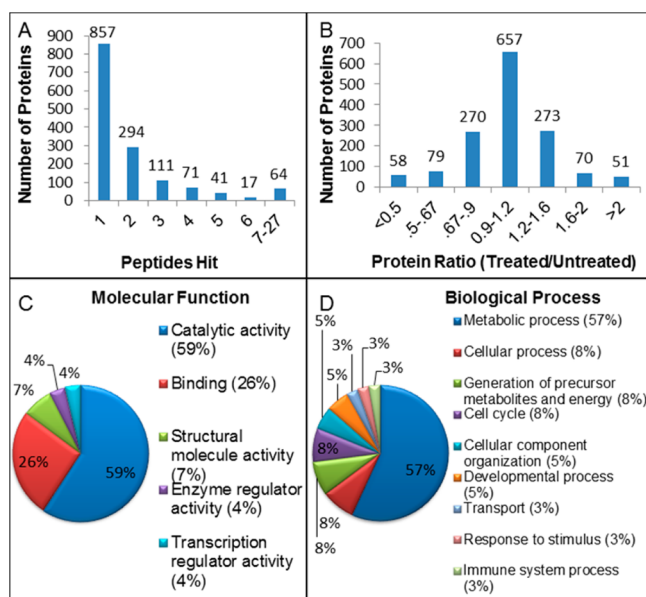
(Table 1). Next, we employed PANTHER (Protein ANnalysis THrough Evolutionary Relationships) to assess the molecular function of the collective proteins and identified catalytic activity and binding as the primary protein function (Figure 2C). Interestingly, using PANTHER to identify the biological processes, cell cycle was scored at 8%, while metabolic process was scored at 57% (Figure 2D). Furthermore, when scored by protein classes, the hydrolase, nucleic acid binding and protease classes were the three highest ranks, respectively. Given the known biological function of Plk1, it would be difficult to predict that Plk1 inhibition would have considerable association with cellular metabolism, nucleic acid binding, and proteolytic activity. Therefore, we sought to further investigate these observations and substantiate our proteomics findings.

BI 6727 Treatment Alters Expression of Multiple Metabolic Proteins

The results of our proteomics analysis have revealed that the inhibition of Plk1 activity results in the decreased expression of multiple metabolic proteins including malate dehydrogenase 1 (MDH1), glutamic-oxaloacetic transaminase 2 (GOT2), and transketolase (TKT). Additionally, we observed a significant reduction in lactate dehydrogenase A (LDHA), confirmed by Western blot (Figure 3A) as well as glucose-6-phosphate isomerase (GPI) and lactate dehydrogenase B (LDHB), which were further assessed at the mRNA level (Figure 3B). Of interest, LDHA, LDHB, and GPI each play an essential role in glycolysis, a metabolic pathway that allows tumor cells to thrive under hypoxic conditions. Glycolysis is an evolutionarily conserved reaction that allows cells to generate ATP from glucose under hypoxic conditions. However, cellular metabolism under normoxic conditions is primarily driven by a much more efficient reaction, mitochondrial oxidative phosphorylation (OXPHOS), yet a hallmark of many cancer cells is their propensity to use the inefficient glycolytic reaction for the production of energy in the presence of oxygen, a phenomenon known as the Warburg effect or aerobic glycolysis.[38] It is interesting to speculate that Plk1 overexpression may contribute to the cancer-related switch from OXPHOS to aerobic glycolysis.

To assess the effect of Plk1 inhibition on aerobic glycolysis, we first measured extracellular levels of lactate, the major byproduct of glucose breakdown. Following a 24 h incubation with BI 6727 under normoxic conditions, there was a significant decrease in lactate levels in both treatment groups (25 nM, 100 nM) when compared with control (Figure 3C). Because these data suggest a disruption in metabolic activity, we next assessed the levels of nicotinamide adenine dinucleotide (NADH) and nicotinamide adenine dinucleotide phosphate (NADPH), the enzymatic cofactors produced during glucose breakdown by glycolysis and the pentose phosphate pathway, respectively. The NADH and NADPH levels were significantly reduced in BI-6727-treated cells, resulting in nearly a five-fold decrease (Figure 3D). To determine if these observations correlate to energy production, we independently measured levels of NAD, an essential coenzyme in ATP production. Interestingly, in addition to the NAD levels being significantly decreased in both the oxidized (NAD^+) and reduced (NADH) forms (Figure 3E), Plk1 inhibition also significantly altered the NAD^+/NADH ratio (Figure 3F). The NAD^+/NADH ratio is considered to be an indicator of the metabolic state and is important in regulating the intracellular redox state, while a shift in the NAD^+/NADH ratio is closely linked to physiological and

Figure 2. Summary of proteomics analysis data. (A) Graphical breakdown representing the number of peptides recognized in all identified proteins. (B) Graphical representation of the calculated protein ratios showing BI 6727-treated samples compared with the vehicle control. (C) Proteins of interest molecular function reported by PANTHER (Protein ANalysis THrough Evolutionary Relationships) as characterized by gene ontology. (D) Proteins of interest biological processes reported by PANTHER as characterized by gene ontology.

corresponding ratio (treated/untreated) (Figure 2B) set as the observational parameters. A secondary data set was then generated using IPA filters set to proteins with more than two identified peptides, no fewer than four hits, and greater than a two-fold change in expression. Another secondary data set was generated using less stringent criteria allowing for one uniquely identified peptide and integrated the IPA connect tool to identify any Plk1-associated proteins with more than four hits and an expression change greater than two-fold. These two analyses resulted in a data set containing 23 proteins of interest

Table 1. Proteins Quantified with Greater than Two-Fold Changes with Unique Peptides, Frames, Hits, and Normalized Ratio Listed[a]

		proteins of interest					
gene	Swiss-Prot ID	protein description	peptides	frames	hits	normalized ratio	fold change
LDHB	P07195	lactate dehydrogenase B chain - LDHB_HUMAN	2	2	18	0.058	−17.24
PPP6R2	O75170	serine/threonine_protein phosphatase 6 regulatory subunit 2 - PP6R2_HUMAN	2	2	17	0.129	−7.75
PSMA3	P25788	proteasome subunit alpha type_3 - PSA3_HUMAN	3	4	17	0.135	−7.41
FBL	P22087	rRNA 2_O_methyltransferase fibrillarin - FBRL_HUMAN	3	4	21	4.862	4.862
SNRPD3	P62318	small nuclear ribonucleoprotein Sm D3 - SMD3_HUMAN	3	3	19	0.22	−4.55
TKT	P29401	transketolase - TKT_HUMAN	12	22	179	0.238	−4.20
GOT2	P00505	aspartate aminotransferase_mitochondrial - AATM_HUMAN	4	4	19	0.318	−3.14
HNRNPC	P07910	heterogeneous nuclear ribonucleoproteins C1/C2 - HNRPC_HUMAN	2	2	26	2.978	2.978
LDHA	P00338	lactate dehydrogenase A chain - LDHA_HUMAN	7	11	145	0.352	−2.84
AHCY	P23526	adenosylhomocysteinase - SAHH_HUMAN	2	3	9	2.531	2.531
RPL10A	P62906	60S ribosomal protein L10a - RL10A_HUMAN	2	3	15	0.398	−2.51
MDH1	P40925	malate dehydrogenase_cytoplasmic - MDHC_HUMAN	10	15	181	0.428	−2.34
GPI	P06744	glucose_6_phosphate isomerase - G6PI_HUMAN	2	2	7	0.439	−2.28
PSMB2	P49721	proteasome subunit beta type_2 - PSB2_HUMAN	5	10	80	0.455	−2.20
JAKMIP2	Q96AA8	Janus kinase and microtubule_interacting protein 2 - JKIP2_HUMAN	6	10	61	0.457	−2.19
HSPA9	P38646	stress_70 protein_ mitochondrial - GRP75_HUMAN	2	1	12	2.158	2.158
PHC1	P78364	polyhomeotic_like protein 1 - PHC1_HUMAN	2	3	21	0.482	−2.07
		polo-like kinase-1-associated genes					
gene	Swiss-Prot ID	description	peptides	frames	hits	normalized ratio	fold change
PSMB6	P28072	proteasome subunit beta type_6 - PSB6_HUMAN	1	1	7	0.18	−5.56
PSMA7	O14818	proteasome subunit alpha type_7 - PSA7_HUMAN	1	3	8	0.406	−2.46
MCM6	Q14566	DNA replication licensing factor MCM6 - MCM6_HUMAN	1	1	4	2.315	2.315
NPM1	P06748	nucleophosmin - NPM_HUMAN	1	3	78	2.277	2.277
TUBB3	Q13509	tubulin beta_3 chain - TBB3_HUMAN	1	1	7	2.118	2.118
CLSPN	Q9HAW4	claspin - CLSPN_HUMAN	1	1	4	2.044	2.044

[a]Proteins identified as having greater than a two-fold change and triggering no less than four separate MS/MS fragmentation scans (hits) of at least two uniquely identified amino acid sequences (peptides) for proteins with no known association to Plk1 or one unique peptide for proteins with a Plk1 association, as identified by ingenuity pathway analysis (IPA). Also included is the number of LC peaks within a well-defined rectangular region in the M/Z versus retention time plane (frames), where each unique peptide was identified.

pathological states.[39,40] Our data suggest a greater decrease in NAD$^+$ following Plk1 inhibition, and given that the pyruvate to lactate conversion is a major route of NAD$^+$ regeneration, it is reasonable to expect that the observed decrease in LDHA is a primary factor in the ratio shift.

Although our data suggest that Plk1 inhibition decreases the metabolic activity of melanoma cells, the question of how Plk1 signaling relates to glycolysis remains to be answered. The initial Warburg hypothesis attributed its effects to dysfunctional OXPHOS; however, recent studies have indicated that OXPHOS remains functional in cancer cells and the shift toward aerobic glycolysis is driven by tumor suppressors such as p53 and PTEN or the oncogenes Ras, C-Myc, and hypoxia-inducible factor-1α (HIF-1α).[41] Plk1 has not only been shown to be involved in p53, PTEN, and C-Myc signaling pathways; recent studies suggest that Plk1 has the potential to act as a mediator between them.[42−44] For example, the loss of PTEN expression is a frequent occurrence in human malignancies and results in elevated phosphoinositide 3-kinase (PI3K) signaling.[45] Recently, Tan et al. have shown that hyperactivation of the PI3K downstream target, PI3K-dependent protein kinase-1 (PDK1), activates Plk1, which in turn stabilizes MYC through direct phosphorylation at Ser-62.[46] While this study has shown a direct connection between two key tumorigenic pathways through Plk1, further correlations can be made when considering the numerous interactions between Plk1 and p53 (discussed later). Given these data, it is interesting to hypothesize that Plk1 overexpression may contribute to the

glycolytic shift described by the Warburg effect; however, further studies are needed to define the role of Plk1 in metabolic signaling.

BI 6727 Treatment Results in the Down-Regulation of Multiple 20S Proteasomal Subunits

The ubiquitin-proteasome system (UPS) plays an integral role in cellular homeostasis through a systematic process that is responsible for 80−90% of intracellular protein degradation.[47] The 26S proteasome is the primary proteolytic complex of the system and is composed of two subcomplexes, the catalytic 20S core particle (CP) and either one or two terminal 19S regulatory particles (RPs). The RPs are responsible for protein capturing by ubiquitin recognition, followed by protein unfolding and translocation to the proteolytic channel of the CP. The CP is made up of four stacked rings, each containing seven α- (α1-7, PSMA1-7) or β-subunits (β1-7, PSMB1-7) in an α−β−β−α configuration (Figure 4A). The outer α-subunits act as a physical barrier to the active β-subunits and create a docking site for the RP, while the inner β-rings are responsible for protein cleavage through caspase-like, trypsin-like, and chymotrypsin-like activities by the catalytically active subunits β1, β2, and β5, respectively.[48]

In our comparative proteomics analysis, we found that BI 6727 treatment results in significant downregulation of multiple 20S subunits in human melanoma cells. Following our IPA analysis, we initially identified subunits α3 and β2 as being 2.20- and 7.41-fold downregulated, respectively. Broadening our IPA
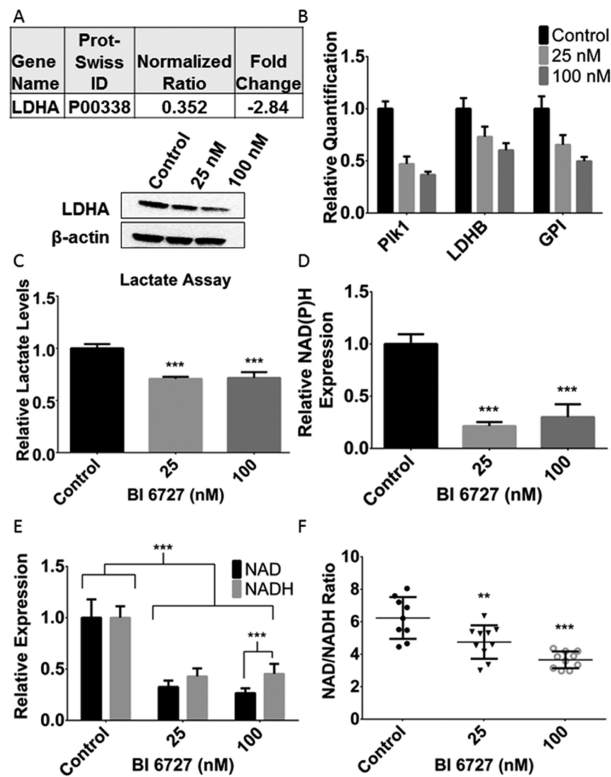
Figure 3. Plk1 inhibition alters cellular metabolism in melanoma cells. (A) Lactate dehydrogenase A (LDHA) protein expression was significantly reduced following Plk1 inhibition in both proteomics (top) and Western blot (bottom) analyses. (B) qPCR analysis suggests a dose-dependent decrease in polo-like kinase 1 (Plk1), lactate dehydrogenase B (LDHB), and glucose-6-phosphate isomerase (GPI) transcript levels following BI 6727 treatment (25 nM, 100 nM). (C) BI 6727 treatment significantly reduces extracellular lactate levels ($p < 0.001$). (D) Plk1 inhibition significantly reduces reduced nicotinamide adenine dinucleotide (NADH) and nicotinamide adenine dinucleotide phosphate (NADPH) levels ($p < 0.001$). (E) NAD and NADH levels are significantly reduced in BI 6727-treated cells when compared with control ($p < 0.001$). (F) NAD/NADH ratio decreases in a BI 6727 dose-dependent manner (** $p < 0.01$, *** $p < 0.001$).
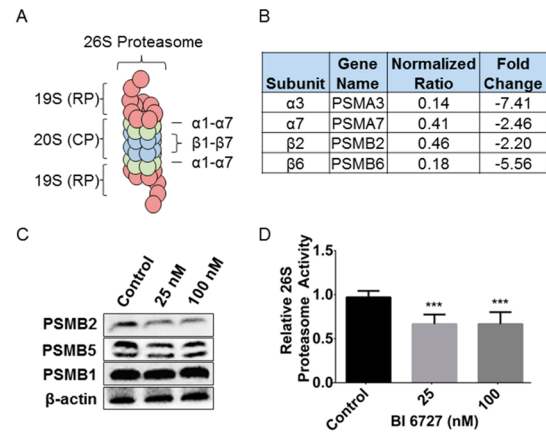

Figure 4. Plk1 inhibition significantly alters 20S proteasome expression and activity. (A) Basic structure of the 20S proteasome. (B) Proteomics analysis identified four 20S proteasome subunits as being down-regulated. (C) Western blot analysis of the catalytically active 20S proteasome subunits, proteasome subunits β2, β5, and β1 (PSMB2, PSMB5, and PSMB1) following Plk1 inhibition. (D) BI 6727-treated cells have significantly decreased 20S proteasome activity ($p < 0.001$).

analysis to include Plk1-associated proteins with only one unique peptide but still having a greater than a two-fold change and no fewer than four hits, we further identified the 20S subunits α7 and β6 as being downregulated by 2.46 and 5.56 fold, respectively (Figure 4B). Because these data suggest that Plk1 inhibition has an effect on a wide range of subunits, we performed a Western blot analysis of the catalytically active subunits β1, β2, and β5 following inhibition of Plk1 by BI 6727 (Figure 4C). We confirmed a decrease in β2, as reported by our proteomics analysis, and additionally observed a modest decrease in β5, while there was no apparent effect on β1. To assess if the decreased subunit expression reflected on proteasome cleavage, we measured 20S proteasome activity using a fluorophore-labeled proteasome substrate. This assay demonstrated a significant reduction in 20S activity in BI 6727-treated cells when compared with control (Figure 4D). These data suggest that Plk1 activity influences proteasome cleavage and is potentially upstream of multiple proteasome subunits in a signaling pathway that has yet to be defined. However, there is evidence of Plk1 indirectly associating with the proteasome through the transcription factors forkhead box M1 (FoxM1) and p53.[49−56]

Similar to Plk1, FoxM1 is overexpressed in numerous human carcinomas and is correlated to poor disease prognosis.[55] Plk1 is involved in a positive feedback loop with FoxM1, where Plk1-dependent phosphorylation is required for efficient FoxM1 activation, which in turn is required for expression of multiple mitotic regulators, including Plk1.[52] Interestingly, proteasome inhibitors have been shown to suppress FoxM1 transcriptional activity, suggesting that proteasome-dependent degradation may confer a level of indirect regulation to Plk1 overexpression in human carcinomas.[50] In addition to FoxM1, the classical tumor suppressor p53 also intersects with both Plk1 and the proteasome. Studies have revealed that Plk1 contributes to p53 repression by directly binding to p53 in addition to phosphorylating GTSE1 and Topors, negative regulators of p53.[42,49,56] Furthermore, Plk1 has also been shown to stabilize the oncoprotein MDM2, an E3 ubiquitin ligase and the principal cellular antagonist of p53.[51] MDM2 mediates p53 protein turnover through constant monoubiquitination, a critical step in the polyubiquitnation of p53 and targeted degradation by the 26S proteasome.[54] Because p53 negatively regulates Plk1, a negative feedback loop exists in the Plk1-p53 axis.[53,57] Considering the findings presented in this study and given the relationships among Plk1, FoxM1, and p53, these data suggest that increased proteasome activity would be conducive to Plk1 overexpression.

Heterogeneous Ribonucleoprotein C1/C2 Is Up-Regulated Following BI 6727 Treatment

The heterogeneous ribonucleoprotein C1/C2 (hnRNPC) is a ubiquitous RNA-binding protein that is expressed in two main isoforms, hnRNPC1 and hnRNPC2.[58] Studies have shown hnRNPC's biological functions to include mRNA transcript packaging, splicing, nuclear retention, and mRNA stability.[59] In this study, we report a significant up-regulation of hnRNPC following Plk1 inhibition, which was confirmed at the protein level by Western blot analysis (Figure 5A). Interestingly, a recent study has shown that hnRNPC overexpression induces micronucleation through the repression of the mitotic protein aurora kinase B (AurkB) in hepatocellular carcinoma (HCC) cells.[60] Using an immunofluorescent nuclear stain, we were able
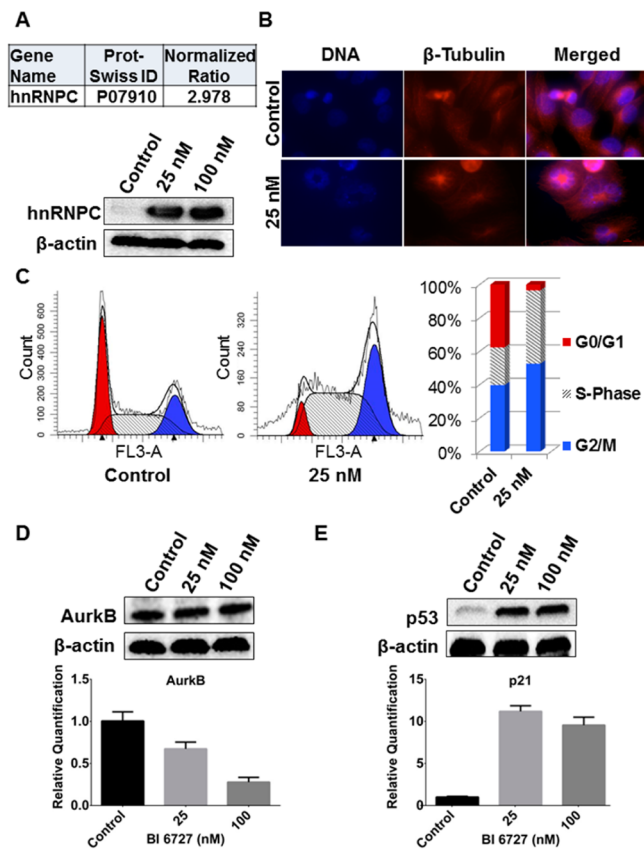
Figure 5. hnRNPC is up-regulated following Plk1 inhibition. (A) Heterogeneous ribonucleoprotein C1/C2 (hnRNPC) protein expression was significantly increased following Plk1 inhibition in both proteomics (top) and Western blot (bottom) analyses. (B) Immunofluorescence microscopy of β-tubulin (red) and Hoecsht DNA (blue) staining, demonstrating micronucleation following Plk1 inhibition. (C) Cell cycle analysis of BI 6727-treated cells demonstrates a pronounced G2/M arrest. (D) Western blot analysis of Aurora kinase B (AurkB) does not indicate significantly altered protein expression following BI 6727 treatment (top), but qPCR analysis reveals decreased mRNA expression levels (bottom). (E) Plk1 inhibition causes a marked increase in p53 protein expression, visualized by Western blot analysis (top) and p53 activity, demonstrated by increased p21 mRNA expression (bottom).

to observe a similar micronucleation phenotype in melanoma cells following Plk1 inhibition (Figure 5B). Next, we wanted to determine if there was also a repression of AurkB. Despite a significant G2/M arrest (Figure 5C), we did not observe any significant changes to AurkB expression at the protein level; however, we did observe a significant reduction in AurkB mRNA (Figure 5D). With the understanding that an accumulation of cells in G2/M would result in increased mitotic proteins such as AurkB and given the consistent protein expression we observed at 24 h, it is possible that we are seeing early evidence of AurkB protein degradation and the reduced transcript levels may be a better indicator of AurkB repression. This evidence suggests that inhibition of Plk1 activity may negatively affect AurkB expression and the mitotic catastrophe associated with Plk1 inhibition may in part be mediated through hnRNPC and AurkB.[9]

Although we have already discussed numerous connections between Plk1 and p53, an additional association exists through hnRNPC. hnRNPC has been shown to enhance p53 translation by directly binding to a cis-element in the 5′ coding region of p53 mRNA.[61] In accordance with these findings, we did find a corresponding increase in p53 protein expression and activity as determined by Western blot and transcriptional analysis of p21, respectively (Figure 5E). These data provide compelling evidence of a novel pathway in Plk1-mediated p53 expression through regulation of hnRNPC. However, the Plk1−p53 axis is a complex signaling network, and extensive studies will be required to determine the role of hnRNPC.

CONCLUSIONS

Inhibition of Plk1 by small-molecule inhibitors has become an extremely active area of research based on the preclinical success of Plk1 inhibition in a wide variety of cancers. While it has been shown in multiple studies that Plk1 inhibition selectively targets cancerous cells over that of their normal counterparts, the molecular mechanisms that contribute to Plk1's selectivity remains poorly understood. Our proteomics study of Plk1 inhibition by BI 6727 in human melanoma A375 cells has revealed the altered expression of multiple proteins that have yet to be identified as part of the Plk1 signaling network. Our proteomics analysis provides evidence of a novel relationship between Plk1 and hnRNPC and that Plk1 inhibition has considerable effect on anaerobic glycolysis and proteasome activity, two pathways that are essential in cancer cell survival. Further studies are needed to determine the significance of these protein interactions, but overall these data provide a solid foundation for novel Plk1 signaling pathways and potential candidates for future targeted therapies.

ASSOCIATED CONTENT

Supporting Information

Table S1. Complete protein list identified by nonunique peptide hits having a protein ratio of a high confidence level ($p < 0.05$), showing Swiss-Prot ID, protein description, number of peptides, frames, hits, and normalized ratio. Table S2. Complete protein list identified by unique peptide hits having a protein ratio of a high confidence level ($p < 0.05$), showing Swiss-Prot ID, protein description, number of peptides, frames, hits and normalized ratio. This material is available free of charge via the Internet at http://pubs.acs.org.

AUTHOR INFORMATION

Corresponding Author

*Tel: (608) 263-5359. Fax: (608) 263-2919. E-mail: nahmad@ wisc.edu.

Author Contributions

The manuscript was written through contributions of all authors. All authors have given approval to the final version of the manuscript.

Notes

The authors declare no competing financial interest.

ACKNOWLEDGMENTS

Schmit for his contributions in the review and preparation of this manuscript.

■ REFERENCES

(1) Sumara, I.; Gimenez-Abian, J. F.; Gerlich, D.; Hirota, T.; Kraft, C.; de la Torre, C.; Ellenberg, J.; Peters, J. M. Roles of polo-like kinase 1 in the assembly of functional mitotic spindles. *Curr. Biol.* **2004**, *14* (19), 1712−1722.

(2) Lane, H. A.; Nigg, E. A. Antibody microinjection reveals an essential role for human polo-like kinase 1 (Plk1) in the functional maturation of mitotic centrosomes. *J. Cell Biol.* **1996**, *135* (6 Pt 2), 1701−1713.

(3) Seong, Y. S.; Kamijo, K.; Lee, J. S.; Fernandez, E.; Kuriyama, R.; Miki, T.; Lee, K. S. A spindle checkpoint arrest and a cytokinesis failure by the dominant-negative polo-box domain of Plk1 in U-2 OS cells. *J. Biol. Chem.* **2002**, *277* (35), 32282−32293.

(4) van Vugt, M. A.; van de Weerdt, B. C.; Vader, G.; Janssen, H.; Calafat, J.; Klompmaker, R.; Wolthuis, R. M.; Medema, R. H. Polo-like kinase-1 is required for bipolar spindle formation but is dispensable for anaphase promoting complex/Cdc20 activation and initiation of cytokinesis. *J. Biol. Chem.* **2004**, *279* (35), 36841−36854.

(5) Gray, P. J., Jr.; Bearss, D. J.; Han, H.; Nagle, R.; Tsao, M. S.; Dean, N.; Von Hoff, D. D. Identification of human polo-like kinase 1 as a potential therapeutic target in pancreatic cancer. *Mol. Cancer Ther.* **2004**, *3* (5), 641−646.

(6) Knecht, R.; Elez, R.; Oechler, M.; Solbach, C.; von Ilberg, C.; Strebhardt, K. Prognostic significance of polo-like kinase (PLK) expression in squamous cell carcinomas of the head and neck. *Cancer Res.* **1999**, *59* (12), 2794−2797.

(7) Mito, K.; Kashima, K.; Kikuchi, H.; Daa, T.; Nakayama, I.; Yokoyama, S. Expression of Polo-Like Kinase (PLK1) in non-Hodgkin's lymphomas. *Leuk. Lymphoma* **2005**, *46* (2), 225−231.

(8) Salvatore, G.; Nappi, T. C.; Salerno, P.; Jiang, Y.; Garbi, C.; Ugolini, C.; Miccoli, P.; Basolo, F.; Castellone, M. D.; Cirafici, A. M.; Melillo, R. M.; Fusco, A.; Bittner, M. L.; Santoro, M. A cell proliferation and chromosomal instability signature in anaplastic thyroid carcinoma. *Cancer Res.* **2007**, *67* (21), 10148−10158.

(9) Schmit, T. L.; Zhong, W.; Setaluri, V.; Spiegelman, V. S.; Ahmad, N. Targeted depletion of Polo-like kinase (Plk) 1 through lentiviral shRNA or a small-molecule inhibitor causes mitotic catastrophe and induction of apoptosis in human melanoma cells. *J. Invest. Dermatol.* **2009**, *129* (12), 2843−2853.

(10) Takahashi, T.; Sano, B.; Nagata, T.; Kato, H.; Sugiyama, Y.; Kunieda, K.; Kimura, M.; Okano, Y.; Saji, S. Polo-like kinase 1 (PLK1) is overexpressed in primary colorectal cancers. *Cancer Sci.* **2003**, *94* (2), 148−152.

(11) Wolf, G.; Elez, R.; Doermer, A.; Holtrich, U.; Ackermann, H.; Stutte, H. J.; Altmannsberger, H. M.; Rubsamen-Waigmann, H.; Strebhardt, K. Prognostic significance of polo-like kinase (PLK) expression in non-small cell lung cancer. *Oncogene* **1997**, *14* (5), 543−549.

(12) Wolf, G.; Hildenbrand, R.; Schwar, C.; Grobholz, R.; Kaufmann, M.; Stutte, H. J.; Strebhardt, K.; Bleyl, U. Polo-like kinase: a novel marker of proliferation: correlation with estrogen-receptor expression in human breast cancer. *Pathol. Res. Pract.* **2000**, *196* (11), 753−759.

(13) Weichert, W.; Denkert, C.; Schmidt, M.; Gekeler, V.; Wolf, G.; Kobel, M.; Dietel, M.; Hauptmann, S. Polo-like kinase isoform expression is a prognostic factor in ovarian carcinoma. *Br. J. Cancer.* **2004**, *90* (4), 815−821.

(14) Strebhardt, K.; Kneisel, L.; Linhart, C.; Bernd, A.; Kaufmann, R. Prognostic value of pololike kinase expression in melanomas. *JAMA, J. Am. Med. Assoc.* **2000**, *283* (4), 479−480.

(15) Weichert, W.; Schmidt, M.; Gekeler, V.; Denkert, C.; Stephan, C.; Jung, K.; Loening, S.; Dietel, M.; Kristiansen, G. Polo-like kinase 1 is overexpressed in prostate cancer and linked to higher tumor grades. *Prostate* **2004**, *60* (3), 240−245.

(16) Hikichi, Y.; Honda, K.; Hikami, K.; Miyashita, H.; Kaieda, I.; Murai, S.; Uchiyama, N.; Hasegawa, M.; Kawamoto, T.; Sato, T.; Ichikawa, T.; Cao, S.; Nie, Z.; Zhang, L.; Yang, J.; Kuida, K.; Kupperman, E. TAK-960, a novel, orally available, selective inhibitor of polo-like kinase 1, shows broad-spectrum preclinical antitumor activity in multiple dosing regimens. *Mol. Cancer Ther.* **2012**, *11* (3), 700−709.

(17) Mross, K.; Frost, A.; Steinbild, S.; Hedbom, S.; Rentschler, J.; Kaiser, R.; Rouyrre, N.; Trommeshauser, D.; Hoesl, C. E.; Munzert, G. Phase I dose escalation and pharmacokinetic study of BI 2536, a novel Polo-like kinase 1 inhibitor, in patients with advanced solid tumors. *J. Clin. Oncol.* **2008**, *26* (34), 5511−5517.

(18) Jimeno, A.; Li, J.; Messersmith, W. A.; Laheru, D.; Rudek, M. A.; Maniar, M.; Hidalgo, M.; Baker, S. D.; Donehower, R. C. Phase I study of ON 01910.Na, a novel modulator of the Polo-like kinase 1 pathway, in adult patients with solid tumors. *J. Clin. Oncol.* **2008**, *26* (34), 5504−5510.

(19) Schoffski, P.; Awada, A.; Dumez, H.; Gil, T.; Bartholomeus, S.; Wolter, P.; Taton, M.; Fritsch, H.; Glomb, P.; Munzert, G. A phase I, dose-escalation study of the novel Polo-like kinase inhibitor volasertib (BI 6727) in patients with advanced solid tumours. *Eur. J. Cancer* **2012**, *48* (2), 179−186.

(20) Olmos, D.; Barker, D.; Sharma, R.; Brunetto, A. T.; Yap, T. A.; Taegtmeyer, A. B.; Barriuso, J.; Medani, H.; Degenhardt, Y. Y.; Allred, A. J.; Smith, D. A.; Murray, S. C.; Lampkin, T. A.; Dar, M. M.; Wilson, R.; de Bono, J. S.; Blagden, S. P. Phase I study of GSK461364, a specific and competitive Polo-like kinase 1 inhibitor, in patients with advanced solid malignancies. *Clin. Cancer. Res.* **2011**, *17* (10), 3420−3430.

(21) Ma, W. W.; Messersmith, W. A.; Dy, G. K.; Weekes, C. D.; Whitworth, A.; Ren, C.; Maniar, M.; Wilhelm, F.; Eckhardt, S. G.; Adjei, A. A.; Jimeno, A. Phase I study of Rigosertib, an inhibitor of the phosphatidylinositol 3-kinase and Polo-like kinase 1 pathways, combined with gemcitabine in patients with solid tumors and pancreatic cancer. *Clin. Cancer. Res.* **2012**, *18* (7), 2048−2055.

(22) Rudolph, D.; Steegmaier, M.; Hoffmann, M.; Grauert, M.; Baum, A.; Quant, J.; Haslinger, C.; Garin-Chesa, P.; Adolf, G. R. BI 6727, a Polo-like kinase inhibitor with improved pharmacokinetic profile and broad antitumor activity. *Clin. Cancer. Res.* **2009**, *15* (9), 3094−3102.

(23) Davies, H.; Bignell, G. R.; Cox, C.; Stephens, P.; Edkins, S.; Clegg, S.; Teague, J.; Woffendin, H.; Garnett, M. J.; Bottomley, W.; Davis, N.; Dicks, E.; Ewing, R.; Floyd, Y.; Gray, K.; Hall, S.; Hawes, R.; Hughes, J.; Kosmidou, V.; Menzies, A.; Mould, C.; Parker, A.; Stevens, C.; Watt, S.; Hooper, S.; Wilson, R.; Jayatilake, H.; Gusterson, B. A.; Cooper, C.; Shipley, J.; Hargrave, D.; Pritchard-Jones, K.; Maitland, N.; Chenevix-Trench, G.; Riggins, G. J.; Bigner, D. D.; Palmieri, G.; Cossu, A.; Flanagan, A.; Nicholson, A.; Ho, J. W.; Leung, S. Y.; Yuen, S. T.; Weber, B. L.; Seigler, H. F.; Darrow, T. L.; Paterson, H.; Marais, R.; Marshall, C. J.; Wooster, R.; Stratton, M. R.; Futreal, P. A. Mutations of the BRAF gene in human cancer. *Nature* **2002**, *417* (6892), 949−954.

(24) Spandidos, A.; Wang, X.; Wang, H.; Seed, B. PrimerBank: a resource of human and mouse PCR primer pairs for gene expression detection and quantification. *Nucleic Acids Res.* **2010**, *38* (Database issue), D792−D799.

(25) Neilson, K. A.; Ali, N. A.; Muralidharan, S.; Mirzaei, M.; Mariani, M.; Assadourian, G.; Lee, A.; van Sluyter, S. C.; Haynes, P. A. Less label, more free: approaches in label-free quantitative mass spectrometry. *Proteomics* **2011**, *11* (4), 535−553.

(26) Old, W. M.; Meyer-Arendt, K.; Aveline-Wolf, L.; Pierce, K. G.; Mendoza, A.; Sevinsky, J. R.; Resing, K. A.; Ahn, N. G. Comparison of label-free methods for quantifying human proteins by shotgun proteomics. *Mol. Cell. Proteomics* **2005**, *4* (10), 1487−1502.

(27) Zhu, W.; Smith, J. W.; Huang, C. M. Mass spectrometry-based label-free quantitative proteomics. *J. Biomed. Biotechnol.* **2010**, *2010*, 840518.

(28) Fedorova, G.; Randak, T.; Lindberg, R. H.; Grabic, R. Comparison of the quantitative performance of a Q-Exactive high-resolution mass spectrometer with that of a triple quadrupole tandem mass spectrometer for the analysis of illicit drugs in wastewater. *Rapid. Commun. Mass. Sp.* **2013**, *27* (15), 1751−1762.

(29) Jones, K. A.; Kim, P. D.; Patel, B. B.; Kelsen, S. G.; Braverman, A.; Swinton, D. J.; Gafken, P. R.; Jones, L. A.; Lane, W. S.; Neveu, J. M.; Leung, H. C.; Shaffer, S. A.; Leszyk, J. D.; Stanley, B. A.; Fox, T. E.; Stanley, A.; Hall, M. J.; Hampel, H.; South, C. D.; de la Chapelle, A.; Burt, R. W.; Jones, D. A.; Kopelovich, L.; Yeung, A. T. Immunodepletion plasma proteomics by tripleTOF 5600 and Orbitrap elite/LTQ-Orbitrap Velos/Q exactive mass spectrometers. *J. Proteome Res.* **2013**, *12* (10), 4351−4365.

(30) Oppermann, F. S.; Klammer, M.; Bobe, C.; Cox, J.; Schaab, C.; Tebbe, A.; Daub, H. Comparison of SILAC and mTRAQ quantification for phosphoproteomics on a quadrupole orbitrap mass spectrometer. *J. Proteome Res.* **2013**, *12* (9), 4089−4100.

(31) Gamez-Pozo, A.; Sanchez-Navarro, I.; Calvo, E.; Agullo-Ortuno, M. T.; Lopez-Vacas, R.; Diaz, E.; Camafeita, E.; Nistal, M.; Madero, R.; Espinosa, E.; Lopez, J. A.; Fresno Vara, J. A. PTRF/cavin-1 and MIF proteins are identified as non-small cell lung cancer biomarkers by label-free proteomics. *PLoS One* **2012**, *7* (3), e33752.

(32) Guillaume, E.; Berger, B.; Affolter, M.; Kussmann, M. Label-free quantitative proteomics of two Bifidobacterium longum strains. *J. Proteomics* **2009**, *72* (5), 771−784.

(33) Lopez, M. F.; Sarracino, D. A.; Vogelsang, M.; Sutton, J. N.; Athanas, M.; Krastins, B.; Garces, A.; Prakash, A.; Peterman, S.; Demirjian, Z.; Inglessis-Azuaje, I.; Feeney, K.; Elia, M.; McMullin, D.; Dec, G. W.; Palacios, I.; Lo, E. H.; Buonanno, F.; Ning, M. Heart-brain signaling in patent foramen ovale-related stroke: differential plasma proteomic expression patterns revealed with a 2-pass liquid chromatography-tandem mass spectrometry discovery workflow. *J. Invest. Med.* **2012**, *60* (8), 1122−1130.

(34) Qu, J.; Lesse, A. J.; Brauer, A. L.; Cao, J.; Gill, S. R.; Murphy, T. F. Proteomic expression profiling of Haemophilus influenzae grown in pooled human sputum from adults with chronic obstructive pulmonary disease reveal antioxidant and stress responses. *BMC Microbiol.* **2010**, *10*, 162.

(35) Sutton, J.; Richmond, T.; Shi, X.; Athanas, M.; Ptak, C.; Gerszten, R.; Bonilla, L. Performance characteristics of an FT MS-based workflow for label-free differential MS analysis of human plasma: standards, reproducibility, targeted feature investigation, and application to a model of controlled myocardial infarction. *Proteomics: Clin. Appl.* **2008**, *2* (6), 862−881.

(36) Tabata, T.; Sato, T.; Kuromitsu, J.; Oda, Y. Pseudo internal standard approach for label-free quantitative proteomics. *Anal. Chem.* **2007**, *79* (22), 8440−8445.

(37) Nilsson, T.; Mann, M.; Aebersold, R.; Yates, J. R., 3rd; Bairoch, A.; Bergeron, J. J. Mass spectrometry in high-throughput proteomics: ready for the big time. *Nat. Methods* **2010**, *7* (9), 681−685.

(38) Koppenol, W. H.; Bounds, P. L.; Dang, C. V. Otto Warburg's contributions to current concepts of cancer metabolism. *Nat. Rev. Cancer* **2011**, *11* (5), 325−337.

(39) Lin, S. J.; Guarente, L. Nicotinamide adenine dinucleotide, a metabolic regulator of transcription, longevity and disease. *Curr. Opin. Cell Biol.* **2003**, *15* (2), 241−246.

(40) Sun, F.; Dai, C.; Xie, J.; Hu, X. Biochemical issues in estimation of cytosolic free NAD/NADH ratio. *PLoS One* **2012**, *7* (5), e34525.

(41) Zheng, J. Energy metabolism of cancer: Glycolysis versus oxidative phosphorylation (Review). *Oncol. Lett.* **2012**, *4* (6), 1151−1157.

(42) Liu, X. S.; Li, H.; Song, B.; Liu, X. Polo-like kinase 1 phosphorylation of G2 and S-phase-expressed 1 protein is essential for p53 inactivation during G2 checkpoint recovery. *EMBO Rep.* **2010**, *11* (8), 626−632.

(43) Liu, X. S.; Song, B.; Elzey, B. D.; Ratliff, T. L.; Konieczny, S. F.; Cheng, L.; Ahmad, N.; Liu, X. Polo-like kinase 1 facilitates loss of PTEN tumor suppressor-induced prostate cancer formation. *J. Biol. Chem.* **2011**, *286* (41), 35795−35800.

(44) Padmanabhan, A.; Li, X.; Bieberich, C. J. Protein Kinase A Regulates MYC Protein through Transcriptional and Post-translational Mechanisms in a Catalytic Subunit Isoform-specific Manner. *J. Biol. Chem.* **2013**, *288* (20), 14158−14169.

(45) Song, M. S.; Salmena, L.; Pandolfi, P. P. The functions and regulation of the PTEN tumour suppressor. *Nat. Rev. Mol. Cell. Biol.* **2012**, *13* (5), 283−296.

(46) Tan, J.; Li, Z.; Lee, P. L.; Guan, P.; Aau, M. Y.; Lee, S. T.; Feng, M.; Lim, C. Z.; Lee, E. Y.; Wee, Z. N.; Lim, Y. C.; Karuturi, R. K.; Yu, Q. PDK1 signaling toward PLK1-MYC activation confers oncogenic transformation, tumor-initiating cell activation, and resistance to mTOR-targeted therapy. *Cancer Discovery* **2013**, *3* (10), 1156−1171.

(47) Shen, M.; Schmitt, S.; Buac, D.; Dou, Q. P. Targeting the ubiquitin-proteasome system for cancer therapy. *Expert Opin. Ther. Targets* **2013**, *17* (9), 1091−1108.

(48) Sahara, K.; Kogleck, L.; Yashiroda, H.; Murata, S. The mechanism for molecular assembly of the proteasome. *Adv. Biol. Regul.* **2014**, *54C*, 51−58.

(49) Ando, K.; Ozaki, T.; Yamamoto, H.; Furuya, K.; Hosoda, M.; Hayashi, S.; Fukuzawa, M.; Nakagawara, A. Polo-like kinase 1 (Plk1) inhibits p53 function by physical interaction and phosphorylation. *J. Biol. Chem.* **2004**, *279* (24), 25549−26661.

(50) Bhat, U. G.; Halasi, M.; Gartel, A. L. FoxM1 is a general target for proteasome inhibitors. *PLoS One* **2009**, *4* (8), e6593.

(51) Dias, S. S.; Hogan, C.; Ochocka, A. M.; Meek, D. W. Polo-like kinase-1 phosphorylates MDM2 at Ser260 and stimulates MDM2-mediated p53 turnover. *FEBS Lett.* **2009**, *583* (22), 3543−3548.

(52) Fu, Z.; Malureanu, L.; Huang, J.; Wang, W.; Li, H.; van Deursen, J. M.; Tindall, D. J.; Chen, J. Plk1-dependent phosphorylation of FoxM1 regulates a transcriptional programme required for mitotic progression. *Nat. Cell Biol.* **2008**, *10* (9), 1076−1082.

(53) McKenzie, L.; King, S.; Marcar, L.; Nicol, S.; Dias, S. S.; Schumm, K.; Robertson, P.; Bourdon, J. C.; Perkins, N.; Fuller-Pace, F.; Meek, D. W. p53-dependent repression of polo-like kinase-1 (PLK1). *Cell Cycle* **2010**, *9* (20), 4200−4212.

(54) Michael, D.; Oren, M. The p53-Mdm2 module and the ubiquitin system. *Semin. Cancer Biol.* **2003**, *13* (1), 49−58.

(55) Wierstra, I. FOXM1 (Forkhead box M1) in tumorigenesis: overexpression in human cancer, implication in tumorigenesis, oncogenic functions, tumor-suppressive properties, and target of anticancer therapy. *Adv. Cancer Res.* **2013**, *119*, 191−419.

(56) Yang, X.; Li, H.; Zhou, Z.; Wang, W. H.; Deng, A.; Andrisani, O.; Liu, X. Plk1-mediated phosphorylation of Topors regulates p53 stability. *J. Biol. Chem.* **2009**, *284* (28), 18588−18592.

(57) Cholewa, B. D.; Liu, X.; Ahmad, N. The role of polo-like kinase 1 in carcinogenesis: cause or consequence? *Cancer Res.* **2013**, *73* (23), 6848−6855.

(58) Burd, C. G.; Swanson, M. S.; Gorlach, M.; Dreyfuss, G. Primary structures of the heterogeneous nuclear ribonucleoprotein A2, B1, and C2 proteins: a diversity of RNA binding proteins is generated by small peptide inserts. *Proc. Natl. Acad. Sci. U. S. A.* **1989**, *86* (24), 9788−9792.

(59) Krecic, A. M.; Swanson, M. S. hnRNP complexes: composition, structure, and function. *Curr. Opin. Cell Biol.* **1999**, *11* (3), 363−371.

(60) Sun, D. Q.; Wang, Y.; Liu, D. G. Overexpression of hnRNPC2 induces multinucleation by repression of Aurora B in hepatocellular carcinoma cells. *Oncol. Lett.* **2013**, *5* (4), 1243−1249.

(61) Christian, K. J.; Lang, M. A.; Raffalli-Mathieu, F. Interaction of heterogeneous nuclear ribonucleoprotein C1/C2 with a novel cis-regulatory element within p53 mRNA as a response to cytostatic drug treatment. *Mol. Pharmacol.* **2008**, *73* (5), 1558−1567.